

DETC2013-13034

ACCURACY ANALYSIS AND VALIDATION OF THE MARS SCIENCE LABORATORY (MSL) ROBOTIC ARM

Curtis L. Collins *

Jet Propulsion Laboratory
California Institute of Technology
Pasadena, CA 91109
Email: Curtis.L.Collins@jpl.nasa.gov

Matthew L. Robinson

Jet Propulsion Laboratory
California Institute of Technology
Pasadena, CA 91109
Email: Matthew.L.Robinson@jpl.nasa.gov

ABSTRACT

The Mars Science Laboratory (MSL) Curiosity Rover is currently exploring the surface of Mars with a suite of tools and instruments mounted to the end of a five degree-of-freedom robotic arm. To verify and meet a set of end-to-end system level accuracy requirements, a detailed positioning uncertainty model of the arm was developed and exercised over the arm operational workspace. Error sources at each link in the arm kinematic chain were estimated and their effects propagated to the tool frames. A rigorous test and measurement program was developed and implemented to collect data to characterize and calibrate the kinematic and stiffness parameters of the arm. Numerous absolute and relative accuracy and repeatability requirements were validated with a combination of analysis and test data extrapolated to the Mars gravity and thermal environment. Initial results of arm accuracy and repeatability on Mars demonstrate the effectiveness of the modeling and test program as the rover continues to explore the foothills of Mount Sharp.

INTRODUCTION

The MSL robotic arm is the seventh articulated arm successfully operated on Mars by NASA. The two Viking landers utilized a translating boom sampling arm in the late 1970s [1], and in 1997 the Pathfinder/Sojourner rover used a deployment mechanism with a passive wrist to place an instrument on a surface

target [2]. True five degree-of-freedom (DOF) articulated motion was provided by the instrument deployment device (IDD) used on the Mars Exploration Rovers (MER) Spirit and Opportunity [3], and the Phoenix lander utilized a four DOF arm and scoop for surface digging and sample delivery [4].

The MER IDD arms were kinematically calibrated using laser tracker metrology [5] with two targets mounted to a stand-in turret [3]. A set of truth "vectors" on the end-effector were generated and used to define an optimum set of kinematic parameters through a least squares fit of a kinematic model that included torsional link stiffness. A similar method was used to calibrate the Phoenix robotic arm [4].

Kinematic calibration of robotic arms is a common and necessary process to ensure good positioning performance. Understanding how error sources impact overall arm accuracy can be performed with a simple kinematic model [6]. Most robot calibration methodologies assume a rigid arm, high accuracy data collection, and some kind of optimization of kinematic parameters [7–9]. Non-geometric parameters such as stiffness are less commonly modeled and used in the calibration process [3, 10].

In what follows, we provide a brief overview of the MSL Robotic Arm along with its positioning requirements. We then discuss the development of the uncertainty model used to analytically support these requirements, and review both the calibration test program and the data analysis used to validate them. We conclude with a brief discussion of the performance of the arm in-situ.

*Address all correspondence to this author.

Arm Layout

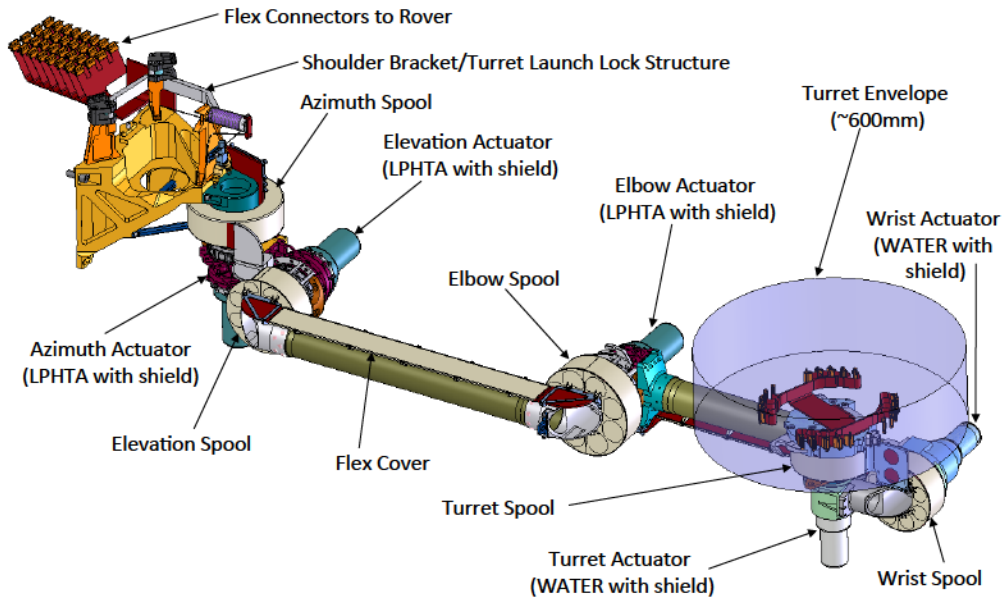


FIGURE 1. ARM LAYOUT

MSL ROBOTIC ARM

The MSL Robotic Arm (RA) has five degrees-of-freedom with the middle three joints parallel to each other and the first and last joints perpendicular to them. The basic layout of the arm is shown in Fig. 1. From base to tool tip, the arm is over 2.1 meters long. This kinematic architecture is sometimes referred to as a Yaw-Pitch-Pitch-Pitch-Yaw (YPPPY) architecture and is similar to that used for the MER IDD [3]. This geometric configuration of joints provides a spherical workspace envelop and eight closed-form inverse kinematics solutions. Joint limits are set such that joint motion cannot cause adjacent links to interfere with each other. In addition, the elevation joint limit is set so that the elbow cannot interfere with driving and effectively eliminates elbow down solutions, thus limiting the number of valid inverse kinematic solutions to four.

Each joint of the arm is powered by a brushless DC motor actuator with a multi-stage planetary geartrain and a brake. The first three joints use one actuator style referred to as the LPHTA, and the last two joints use another referred to as the WATER. Table 1 shows the basic high level specifications of each actuator type. The maximum output torque for each actuator family is based on current limiting control to 5A and 3A for the LPHTA and WATER actuators respectively, on a nominally 28V bus. Each joint has a known backlash at the output. Joint position is measured on the motor side by encoders and on the output side by resolvers.

Customized flex cable runs from the shoulder of the arm, around each joint, and ends at the turret interface bringing power to the actuators, heaters, turret tools and instruments, and sensing

TABLE 1. LPHTA AND WATER ACTUATOR SPECS

Parameter	Units	LPHTA	WATER
Gear Ratio	none	7520	4624
Max Output Torque	Nm	1143	259
Max Current Limit	A	5	3
Backlash	mrad	3.64	4.36
Mass	kg	7.8	4.24

lines back to the rover processors. The mass of the arm from shoulder bracket to turret interface is ~65kg. The mass of the flex cable alone is larger than either the MER IDD or the Phoenix RA. For additional design details, see [11].

Mounted to the end of the robotic arm is a ~30kg turret composed of a powdering drill, a brush, a microscopic imager, a spectrometer, and a scooping and sample processing device. See Fig. 2. For the purposes of kinematic calibration, what is important about the turret is that it has a precision interface with the robotic arm, and a set of well-defined tool frames. Kinematic frames will be described in more detail in a later section.

At the base of the robotic arm is a shoulder bracket that provides mounting points to the front panel of the Curiosity rover as well as stow restraints to support the turret during launch, landing, and driving activities. The final dimensions of the arm were driven by a trade between packaging for stow, reachability over a primary workspace in front of the rover, and access to hardware on the front panel and top deck of the rover.

The primary workspace of the arm is an 80 cm diameter 100

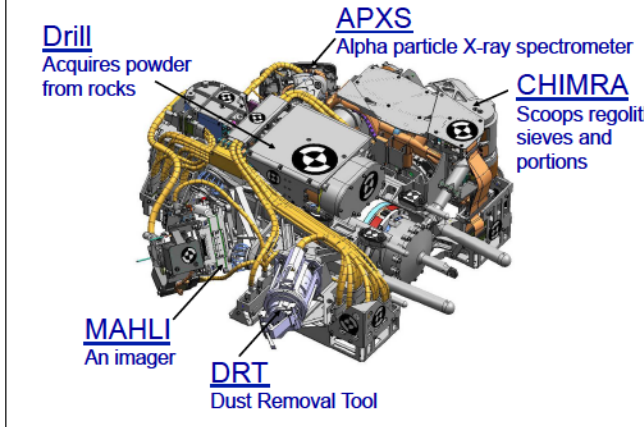


FIGURE 2. TURRET

cm tall cylinder located 110 cm in front of the rover and is positioned to extend 20 cm below the nominal ground plane. The arm is designed to perform sampling and science operations anywhere within this cylinder, shown in Fig. 3. Targets in front of the rover are identified by stereo imagery which constrains the set of possible surface normals that can be resolved. Because of this, the arm is designed to align tools within what we call a wedge of approach vectors that extend from horizontal to vertical, and ± 45 degrees side to side.

Positioning Requirements

The RA has five primary and numerous secondary functional requirements. The primary functions the arm must support are:

1. Contact Science: the arm must place instruments on targets in the primary workspace with a prescribed accuracy and repeatability
2. Sampling: the arm must place a drill on a target in the primary workspace and preload it to 300N
3. Sample Processing: the arm must control the flow of sample over sieves and through chambers by controlled motions with respect to gravity
4. Sample Delivery: the arm must precisely position a portion tube above instrument inlets while accounting for gravity
5. Bit Exchange: the arm must precisely dock with and load a bit box in support of autonomous bit exchange

The key system requirements on the positioning performance of the robotic arm are as follows. The maximum total position error shall be ± 20 mm. The maximum total placement error (or lateral position error) shall be ± 15 mm. The repeatability shall be less than ± 10 mm. The system shall accommodate the freespace positioning of instruments at rover tilts up to 30° . The system shall accommodate sampling activities (preload, drilling, and processing) at rover tilts up to 20° .

Operational Deployment

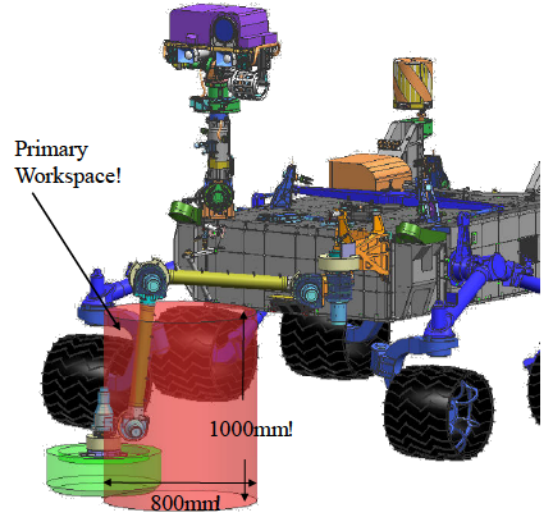


FIGURE 3. PRIMARY WORKSPACE

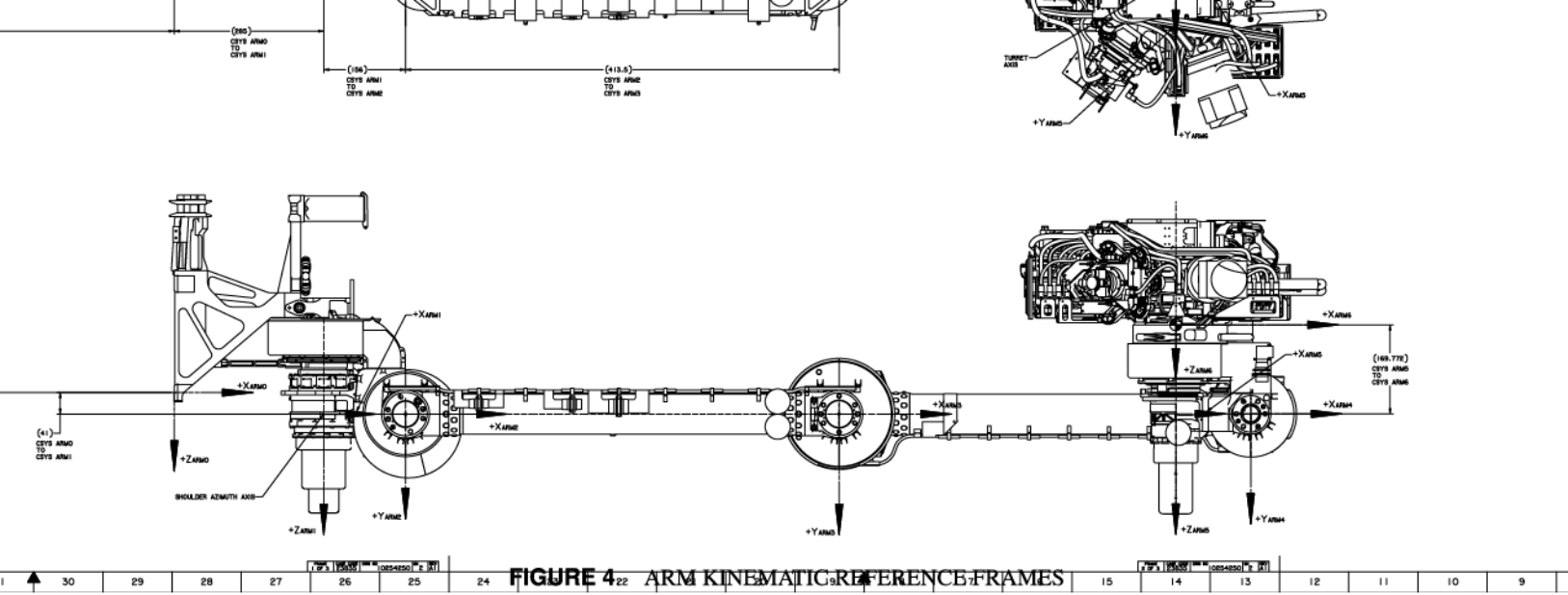
Numerous characteristics worked against being able to both satisfy the functional requirements and achieve the accuracy requirements. They include joint backlash, mass constraints, volume constraints, stiffness properties driven by launch, landing, and driving dynamics, large ambient temperature swings, and an inability to calibrate the system in a low gravity environment. To deal with the variety of uncertainties in the system and their potential impact on arm performance, we developed a detailed model of the arm kinematics and statics, and used it to both predict the effects of uncertainty on arm accuracy and repeatability and to understand the driving uncertainties. This allowed us to develop a calibration and test program as well as data reduction strategies to minimize the accumulation of known errors, and bound, as much as practical, the unknown errors.

UNCERTAINTY ANALYSIS

In this section we provide a brief overview of the arm kinematic, statics, and deflection model which we use in its differential form to analyze how different types of errors at different points along the arm impact arm accuracy and repeatability. We identify various sources of error from the rover and arm structure, arm actuators and arm avionics, and provide a basis of estimate for them. We then discuss how those errors are propagated to define arm tool frame errors.

Arm Kinematic, Static, and Deflection Model

A detailed kinematic, static, and deflection model of the arm was formulated for both the operational loads analysis and the uncertainty analysis. Like any kinematic model, we begin by defining a set of link and tool reference frames along the lines of the Denavit-Hartenberg convention [12], but deviating where



hardware features or other conventions support a more natural frame placement. See, for example, the frames defined in Fig. 4. We use a general homogeneous link transformation defined by a sequence of pure rotations and translations as follows.

$${}^{j-1}D_j = R_z(\theta)T_z(d)R_y(\beta)T_y(b)R_x(\alpha)T_x(a) \quad (1)$$

where ${}^{j-1}D_j$ represents the location of frame j with respect to frame $j-1$, and $\theta, d, \beta, b, \alpha, a$ are the kinematic parameters of the link. The forward kinematics is then represented as

$${}^{rvr}D_{Tool} = \prod_{j=rvr}^{Tool} {}^{j-1}D_j \quad (2)$$

We then construct what we call the frame Jacobian (with a screw-based representation) for each frame by extracting the rotation matrix R and translation vector p from the homogeneous transformation and constructing the following 6×6 matrix

$${}^{j-1}J_j = \begin{bmatrix} {}^{j-1}R_j & 0 \\ [{}^{j-1}P_j] & {}^{j-1}R_j \end{bmatrix} \quad (3)$$

where j is an index representing what frame we are working in and $[{}^{j-1}P_j]$ is the 3×3 skew-symmetric matrix formed from the translation vector p . We use J_j in both the statics and deflection models.

The total set of reaction forces at each frame can be represented as

$$\tau_j = J_j^T \tilde{W}_j \quad (4)$$

Where J_j is the frame Jacobian, \tilde{W}_j is the sum of the forces acting on the frame (including gravity forces). The deflection T under

load at each frame can be written as

$$T_j = J_j C_j \tau_j \quad (5)$$

Where C_j is the 6×6 compliance matrix for link j . Finally, a thermal deflection U at each frame can be written as

$$U_j = J_j V_j \Delta t \quad (6)$$

where V_j is a vector of coefficients of thermal expansion of each link and Δt is the temperature change. The total deflection of the arm can be written as the sum of the local deflections as long as the screws are all represented in the same reference frame. See [12–14] for the relevant background on kinematics and screw theory used in these models.

Error Sources

The starting point for the RA error analysis is a set of error sources and error magnitude estimates. Table 2 shows the alphabetical list of primary error sources considered in this analysis along with a brief description and classification of the error as systematic or random.

The approach we have taken for estimating values for the errors is to look at their effects on each distinct link of the RA kinematic chain. The basic idea is that there is one key coordinate frame on each link. Errors are thought of as leading to small rotations about the coordinate frame axes and small translations along the coordinate axes. All error values are expressed as uncertainties (i.e. \pm value).

For the purposes of this analysis, we roll up all structural and modeling errors from the rover to azimuth joint and express them in *Arm1*. Similarly we roll up structural and modeling errors from the turret interface frame, *Arm6*, to the tool frame and express them in the appropriate tool frame, *Tool*. For source errors associated with the actuators, we express the errors in the appropriate link frames from *Arm1* to *Arm5*.

TABLE 2. SUMMARY OF ERROR SOURCES

Source Name	Description	Type
Assembly	Assembly knowledge error (kinematic parameter knowledge)	Systematic
Backlash	Freeplay in the actuator transmission due to gear mesh	Random
Deflection	Uncompensated deflection due to stiffness model uncertainty	Systematic
Distortion (Bulk)	Uncompensated distortion due to bulk thermal model uncertainty	Systematic
Distortion (Grad)	Unmodeled distortion due to thermal gradients	Systematic
Encoder	Control error due to 10 quadrature encoder counts	Random
Slop	Freeplay in the mechanical assembly	Random
Windup	Torsional deflection of the gear-train due to internal friction	Random
Wobble	Precession and nutation of joint axis due to bearings	Random
Zero Offset	Error in zero position knowledge due to hard stop calibration. Zero offset error is a function of current and torque uncertainty	Random

Systematic Sources. By systematic errors we mean errors that are basically repeatable under the same set of environmental conditions. These errors effect accuracy results, but have lesser or no effect on repeatability results. Their impact is dependent on how well we can model them and how much we can compensate for them. The systematic errors are listed in Tab. 2.

Assembly errors represent the build up of dimensional error in the links that define the basic kinematics of the arm. For stiff arms in controlled temperature environments, this is the primary source of error that is the target of kinematic calibration.

However, for a relatively compliant arm operating in a Mars environment, errors in the stiffness model lead to deflection compensation errors, and errors in the thermal model lead to thermal compensation errors. In addition, some thermal deflection due to temperature gradients in the hardware cannot effectively be modeled, but only bounded. Based on our experience with deflection and thermal models, we assumed we could compensate for gravity deflection errors within 20% and bulk thermal distortion errors within 50%. These turned out to be conservative bounding estimates of these error sources.

Random Sources. Random errors are errors that are not repeatable and can take on any value between some bounds. We cannot compensate for random errors, and in general, their exact value is not known. All of the random sources of error are associated with the actuators and the interfaces between the actuators and the link structure.

With the exception of slop and wobble, which are estimated to be very small, the random error sources listed in Tab. 2 are actuator level sources that effect our knowledge and control of the arm joint angles. Backlash, encoder, windup and zero-offset errors all add together to produce a resultant uncertainty in joint

position. What is interesting to note is that for an arm of this size, 1 mrad of error in any joint position leads to $\sim 1\text{-}2$ mm errors in tool position. Because of this, we developed (and ultimately implemented) a backlash compensation strategy and a process to improve the accuracy and repeatability of our hard-stop calibration and incremental encoder initialization. We will discuss these in more detail in a later section.

Propagating Source Errors

As discussed in the last section, error sources are defined as causing small rotational and translational displacements about individual coordinate frames in the kinematic chain. These small displacements propagate to errors in the position and orientation of a tool frame. How individual errors propagate is dependent upon the pose of the arm. Using the coordinate transformations defined for each link, we construct the mapping between components of the source errors to propagated errors at the tool frame as follows.

First we transform ${}^{j-1}J_j$ into a common tool frame to get the set ${}^{Tool}J_j$. Then, for a given source error vector at a given frame, we can represent the tool frame error as

$$u_{j,i} = J_j \theta_{j,i} \quad (7)$$

where the first subscript j denotes the frame under consideration and the second subscript i denotes the error source. We have dropped the *Tool* superscript for convenience. The first three components of $u_{j,i}$ represent the angular errors at the tool frame caused by the i -th source at the j -th frame, and the last three components of $u_{j,i}$ represent the translational errors at the tool frame. $\theta_{j,i}$ is the 6 vector of error source components

$$\theta_{j,i} = (r_x, r_y, r_z, t_x, t_y, t_z)_{j,i}^T$$

where r_x, r_y, r_z are the small rotations and t_x, t_y, t_z are the small translations caused by the i -th source at the j -th frame.

Deflection due to gravity is a function of arm pose and the gravity vector. Given the magnitude and direction of the acceleration due to gravity and the pose of the arm (joint angles) we can compute the forces and moments caused by gravity in each coordinate frame j . We can then represent the deflection of the j -th reference frame using a 6×6 compliance matrix C_j as

$$\theta_{j,deflection} = C_j g_j \quad (8)$$

where $g_j = \{f_j, m_j\}$ is the vector of gravity forces and moments. We represent the uncompensated deflection at the tool due to deflection at the j -th frame as

$$u_{j,deflection} = \epsilon_s J_j \theta_{j,deflection} = \epsilon_s J_j C_j g_j \quad (9)$$

where ϵ_s is the percent uncertainty in the stiffness model (0 percent means perfect compensation, while 100 percent means no compensation).

Bulk thermal distortion is a function of the change in temperature from Earth ambient (where the kinematic calibration was performed). We represent the uncompensated distortion at the tool due to distortion at the j -th frame as

$$u_{j,distortion} = \epsilon_t J_j V_j (\Delta t)$$

where ϵ_t is the percent uncertainty in the thermal model, V_j is a thermal expansion vector corresponding to the appropriate link, and Δt is the change in temperature in degrees Celsius.

We are currently tracking $n = 7$ reference frames and $m = 10$ sources error in the end-to-end accuracy analysis. The propagated errors can be combined to produce a total error budget in a variety of ways.

For notational convenience we define an ordered array of coordinate frames (whose elements are denoted by j)

$$\{Arm1, Arm2, Arm3, Arm4, Arm5, Arm6, Tool\}$$

and an ordered array of error sources (whose elements are denoted by i)

$$\{assembly, grad\ distortion, encoder, slop, windup\ wobble, zero\ offset, backlash, deflection, distortion\}$$

We can now define three combined error cases.

To get the worst case error bounds we add all the errors together. For a single source, we can add all the results from each frame together. Then we can add all the source results together to get

$$u_{total} = \sum_{i=1}^m \sum_{j=1}^n s_{j,i} u_{j,i} \quad (10)$$

where $s_{j,i}$ is either 0 or 1 depending if whether we include that particular propagated error in the total. This allows us to turn on/off errors as needed.

To get the best case total error we take the root sum square (RSS) of all the errors together. For a single source, we can RSS the results from each frame together. Then we can RSS all the source results together.

$$u_{total} = \sqrt{\sum_{i=1}^m \sum_{j=1}^n (s_{j,i} u_{j,i})^2} \quad (11)$$

A conservative yet balanced approximation of the error is a combination of the sum of errors and the RSS of errors. For this analysis, for each source we add the contribution of each frame to get a source error.

$$u_i = \sum_{j=1}^n s_{j,i} u_{j,i} \quad (12)$$

For the results presented here, we add the results of backlash, uncompensated deflection and uncompensated distortion to the RSS of all the other sources. The argument is that backlash is not truly random and will likely be on the outer limits of the range. Deflection and distortion uncertainties are a systematic and could always lie on their outer limits.

$$u_{total} = \sqrt{\sum_{i=1}^{m-3} u_i^2 + u_{backlash} + u_{deflection} + u_{distortion}} \quad (13)$$

Analytical Results

The initial motivation for developing the arm uncertainty model was to understand the sensitivity of the arm accuracy and repeatability to source errors and to determine whether or not the requirements were realistic. For arm accuracy studies we included all error sources, assumed a 20% deflection compensation error, a 50% thermal compensation error with a 100C temperature change, and exercised the model over a set of ~15000 arm poses in the primary workspace. For arm repeatability studies, we excluded the effects of assembly, backlash, deflection, windup and zero offset errors, and reduced the errors due to thermal changes for activities that occur together on the same day (for example, tool change). We again exercised the model over a set of ~15000 arm poses in the primary workspace. A comparison of requirements and estimated workspace component errors are shown in Tab. 3. The estimated budgets use three sigma values in all cases.

TABLE 3. ACCURACY/REPEATABILITY REQUIREMENTS AND BUDGETS

Component	Required Value	Estimated Budget
Total Position Accuracy	±20 mm	±26.2 mm
Lateral Position Accuracy	±15 mm	±23.2 mm
Axial Orientation Accuracy	±9.8°	±1.2°
Lateral Position Repeatability	±10 mm	±11.2 mm
Normal Position Repeatability	±10 mm	±7.2 mm
Axial Orientation Repeatability	±2°	±0.7°

While the preceding analysis gave what we believe to be reasonable, traceable bounds on the position errors, it also revealed ways to improve the system level performance of the arm. It was clear that thermal compensation, even with a large uncertainty in the model helped to reduce errors on the order of millimeters. The two other significant sources were rover stiffness uncertainty and zero offset uncertainty, both of which could be improved by testing and careful procedures. Rover stiffness was characterized on the engineering rover model specifically for arm based loads. Zero offset uncertainty was also expected to be improved using as-built actuator and current sensing parameters. Additional improvements in accuracy were also achieved using backlash compensation and relative deflection compensation control modes being implemented in flight software. In the end, a successful calibration test program and data reduction both validated and proved the conservatism in our models.

ARM PARAMETER CALIBRATION

The Flight Model (FM) robotic arm was designed, assembled and unit-tested by MDA Robotics (formerly Alliance Space Systems, Inc.). The unit was delivered to the Jet Propulsion Laboratory for integration, system level testing, and calibration. Calibrating the MSL robotic arm required four key steps:

1. Detailed test planning
2. Test execution and data collection
3. Data processing and parameter optimization
4. Calibration parameter verification

Kinematic Calibration Data Collection

The general philosophy for developing the test plan for arm calibration was to collect position and orientation data for multiple arm poses (including poses from different inverse kinematic branches) over the primary workspace, with multiple loading conditions to exercise the stiffness and deflection model. Analysis had shown that calibrating the fully integrated arm and turret system in Earth gravity would require moderate to heavy loads that would limit the life of the actuators as well as cause deflections larger than what would be seen on Mars. Because of this, two light weight turrets were designed to accommodate multiple Spherically Mounted Retroreflector (SMR) nests to allow the 6 DOF position and orientation of the turret to be measured by a laser tracker [5], while reducing loads on the actuators and providing deflections more in line with Mars operations.

The key to being able to design and integrate a stand-in turret with multiple mass configurations was the well-defined precision turret mounting interface. In the end, 8 kg and 19 kg stand-in turret hardware (see Fig. 5) was used to collect calibration data in addition to verification data ultimately collected with the 30 kg full-mass integrated turret. Even multiple turret masses were not enough to fully exercise the stiffness model under gravity with

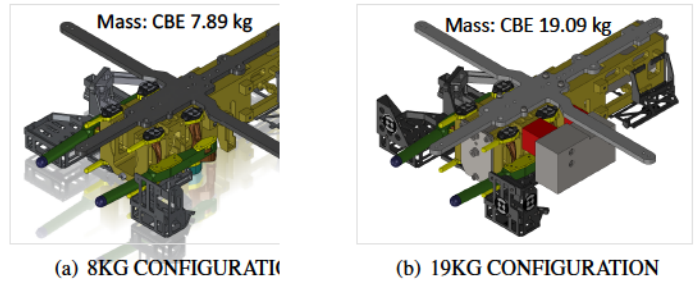


FIGURE 5. FM ARM LIGHTWEIGHT TURRETS

the rover on flat ground, so a tilt table was designed to roll the rover to 20 degrees to apply loads equivalent to a greater than 30 degree roll on Mars.

With the general plan in place, a detailed procedure was developed so that when the time came to execute the test in the Spacecraft Assembly Facility (SAF) cleanroom, it would run smoothly and efficiently. Detailed plans for setting up SMRs to measure the rover base frame, ground reference frame and turret frame from any orientation were outlined. 160 arm poses were chosen from a set of randomly generated poses over the primary workspace. Approximately 30 percent of the poses used a shoulder-in kinematic configuration while the remaining 70 percent used a shoulder-out kinematic configuration. The 160 poses were further broken down into 4 groups of 40 poses. The first two groups of poses were to be run with the two light weight turrets with the rover on level ground. The second two groups of poses were to be run with two light weight turrets with the rover on its 20 degree roll table. Each time the arm was to be posed, the laser tracker would be used to measure the locations of the ground, rover, and turret mounted SMRs.

A critical part of the calibration process was performed even before the calibration data collection began. This involved the initialization of the incremental encoders. On all JPL flight arms, including MSL, encoders are initialized through hardstop calibration, that is, by running a joint into one of its hardstops until it stalls, thus defining its position within some small uncertainty. To maximize the repeatability of the hardstop calibration of the MSL arm in the event it might have to be performed on Mars, a special no-turret configuration of the arm was used. Analysis was performed with the arm with no turret on Earth, and with the turret on Mars. Arm configurations were planned that provided both access to the hardstops and equivalent torques between the Earth and Mars poses and configurations. In this way, the total load and windup on the actuator would be as repeatable as possible. In addition, each joint was calibrated against its negative hardstop to put each actuator in the same initial backlash state to ensure a standard relationship between encoder position, joint loading, and future backlash states necessary for backlash state estimation and compensation.

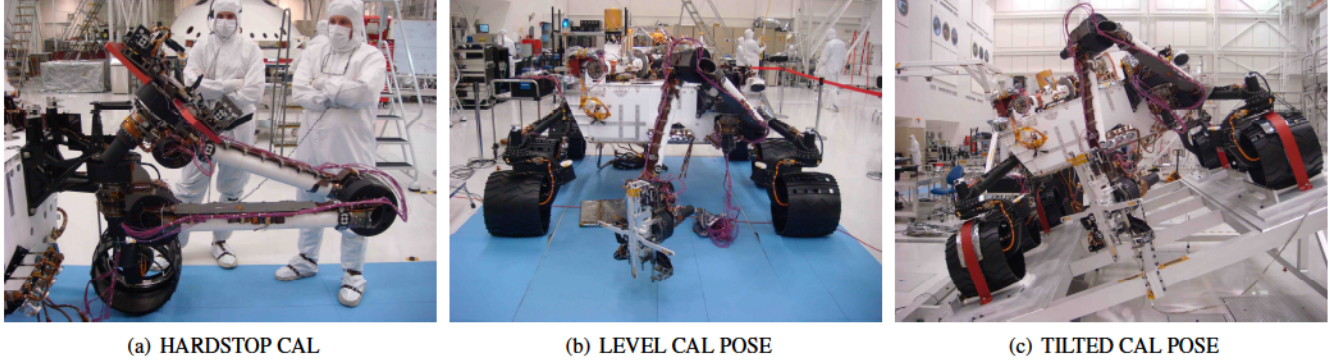


FIGURE 6. FM ARM CALIBRATION TESTING

Once the plan was in place and the procedures written, the whole process was executed with the flight hardware in SAF. Many teams were involved in the test, including the systems team which sent the arm motion commands and monitored the telemetry, the mechanical team which helped reconfigure the turret hardware and ultimately lifted the entire rover onto the tilt platform, the metrology team that set up the laser tracker, placed and measured the SMR locations, and logged the data, and last but not least, the arm team that coordinated the whole activity. Figure 6 shows some key highlights of the test. The calibration test was run over 8 shifts on 4 consecutive days. With that, the first two steps in the process were completed in September 2010.

Calibration Data Processing

Raw metrology data consisting of coordinates of rover and turret mounted targets was processed as follows. First the location of the rover and the turret frame were constructed from the corresponding visible measured targets. Then rover frame motion was factored out and the resulting rover to turret position and orientation was computed for each arm pose.

For each pose, we assume that

$$D_{modeled} D_{error} = D_{measured} \quad (14)$$

where

$$D_{modeled} = D_{rigid} D_{deflected} \quad (15)$$

Then we compute the error as

$$D_{error} = D_{modeled}^{-1} D_{measured} \quad (16)$$

Since D_{error} represents a small displacement, we convert it to a screw representation denoted $T_{error} = \{\omega, v\}$, with magnitude

$$|T_{error}| = \sqrt{w_1 \omega^2 + w_2 v^2} \quad (17)$$

where w_1 and w_2 are weighting factors.

We formulate the calibration equations by constructing the following linear system where i is taken over the number of poses and j is taken over the set of kinematic frames.

$$T_{error,i} = [J_i] \dot{\theta}_{kin} \quad (18)$$

where

$$[J_i] = [J_{Arm1} J_{Arm2} J_{Arm3} J_{Arm4} J_{Arm5} J_{Arm6} J_{Tool}] \quad (19)$$

$$\dot{\theta}_{kin} = \{\dot{\theta}_{Arm1} \dot{\theta}_{Arm2} \dot{\theta}_{Arm3} \dot{\theta}_{Arm4} \dot{\theta}_{Arm5} \dot{\theta}_{Arm6} \dot{\theta}_{Tool}\}^T \quad (20)$$

and

$$\dot{\theta}_j = \{r_x r_y r_z t_x t_y t_z\}_j^T \quad (21)$$

The calibration problem then becomes one of solving the following for $\dot{\theta}_{kin}$.

$$\begin{Bmatrix} T_1 \\ T_2 \\ T_3 \\ \vdots \\ T_n \end{Bmatrix} = \begin{Bmatrix} J_1 \\ J_2 \\ J_3 \\ \vdots \\ J_n \end{Bmatrix} \dot{\theta}_{kin} \quad (22)$$

Figure 7 shows the total position and orientation errors before and after the calibrated parameters were applied. In each case, we generally saw a factor of five improvement in accuracy. It is interesting to note that the four clusters of poses with higher than average errors before the calibration correspond to shoulder-in poses where multiple joints fell to the other side if their backlash from their initialized states. Backlash state prediction was included as part of the deflected pose estimate and consistently helped reduce backlash related errors.

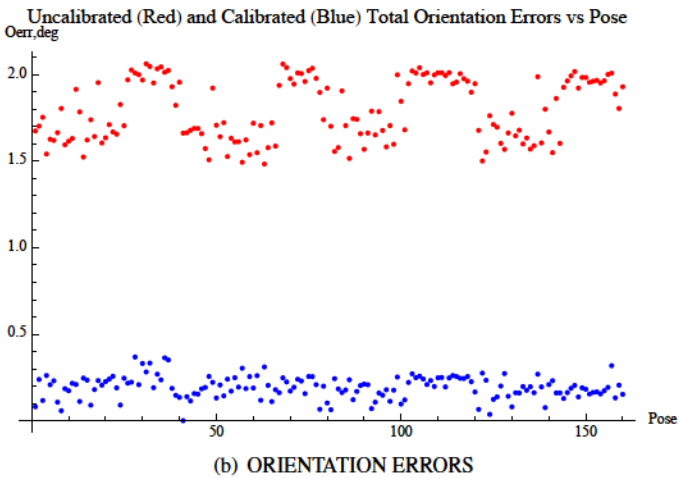
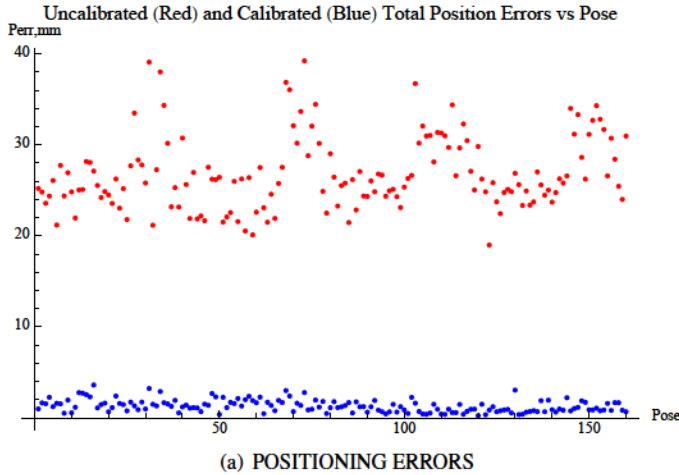


FIGURE 7. UNCALIBRATED AND CALIBRATED ERRORS

Verification and Projections for Mars

The final step in the calibration process was an Earth based verification of the calibrated parameters and zero-offsets. The zero-offsets were applied to the flight system at the encoder level, and the hardstop locations were updated with the same corresponding offsets. Then, after being integrated with the full-mass turret, the arm was commanded to move to a set of turret frame positions with deflection and backlash compensation. The turret location was again measured using SMRs glued on the flight turret hardware and registered with special set of targets on the turret interface plate. The results were statistically equivalent to the initial calibration results, demonstrating Earth-based arm accuracy of less than 5mm.

In order to predict the final expected accuracy and repeatability results for the turret tools and instruments on Mars, we needed to add in additional error sources that would effect performance on Mars. These sources included orientation induced position errors at the tool frames, instrument isolator hystere-

sis, thermally induced errors (due to the residual uncertainty in the model and the un-modeled gradient distortions), deflection compensation errors due to residual errors in the stiffness model, and motor controller errors due to final tuned motor parameters. With these error accounted for, our final predicted accuracy and repeatability on Mars was shown to satisfy our requirements and are summarized in Tab. 4.

TABLE 4. ACCURACY/REPEATABILITY REQUIREMENTS AND ESTIMATES FOR MARS

Component	Required Value	Estimated Value
Total Position Accuracy	± 20 mm	± 14.0 mm
Lateral Position Accuracy	± 15 mm	± 12.7 mm
Axial Orientation Accuracy	$\pm 9.8^\circ$	$\pm 1.1^\circ$
Lateral Position Repeatability	± 10 mm	± 7.7 mm
Normal Position Repeatability	± 10 mm	± 5.0 mm
Axial Orientation Repeatability	$\pm 2^\circ$	$\pm 1.0^\circ$

PERFORMANCE ON MARS

The first instrument placement on Mars took place on Sol 46 when the APXS instrument was placed in contact with surface target Jake Matijevic, named for the late systems engineer who made pioneering contributions to every rover surface mission at JPL. Figure 8 shows the arm unstowed and in its staging pose ready for placement, the rock target before placement, and the arm with its microscopic imager in close proximity to the target after a relative tool change move from APXS contact. This set of motions qualitatively and successfully demonstrated the system end-to-end accuracy and repeatability to be operationally acceptable and consistent with predictions.

CONCLUSIONS

The MSL robotic arm was designed with both high accuracy and low stiffness as competing requirements. A detailed uncertainty model of the arm along with bounding estimates of source errors provided conservative predictions of arm performance and provided insight into the sensitivity of key parameters. Detailed arm calibration test planning, careful test execution, rigorous calibration data analysis, and followup hardware verification testing resulted in a final calibrated parameter set and validated model that demonstrated effective arm positioning performance. System level performance is still being evaluated on Mars with each set of target placement activities providing additional data that is being assessed. The operational accuracy and repeatability of the system continues to be refined as Curiosity slowly climbs Mount Sharp in search of evidence of habitability.

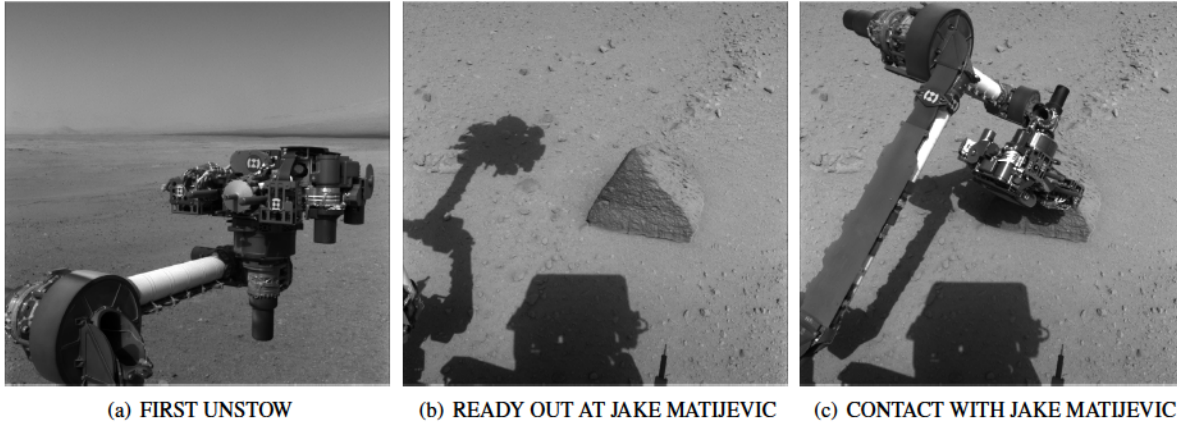


FIGURE 8. FM ARM ON MARS

ACKNOWLEDGMENT

The arm modeling and calibration effort owes its success to many dedicated colleagues at JPL and its contractors. Brett Kennedy, Ken Smith (MDA Robotics), Steve Peters, Rick Welch, Joe Melko, Chris Voorhees (Planetary Resources, Inc.), and Louise Jandura contributed to the uncertainty model and error estimates. The calibration test campaign involved over 100 hours of testing and was supported by Rick Redick, Chris Leger, and Joseph Carsten as well as numerous ATLO and Testbed support personnel. Nine versions of the stand-in turret were designed and delivered by Ken Glazebrook. Scott Mathews designed and delivered the rover tilt fixture, and Nathaniel Thompson designed and delivered the testbed hexapod. Metrology procedures and data collection would not have run so smoothly without the efforts of Paul Lytal, Gene Poyorena, and Jerry Clark. Daniel Limonadi coordinated whole test effort as SSS Phase Lead. The work described in this paper was carried out at the Jet Propulsion Laboratory, California Institute of Technology, under a contract with the National Aeronautics and Space Administration.

REFERENCES

- [1] Holmberg, H. A., Faust, R. P., and Holt, H. M., 1980. Viking '75 Spacecraft Design and Test Summary, Volume 1 - Lander Design. NASA Reference Publication 1027 N81-10100, National Aeronautics and Space Administration (NASA).
- [2] Rover-Team, 1997. "The Pathfinder microrover". *Journal of Geophysical Research*, **102**(E2), Feb., pp. 3989–4001.
- [3] Baumgartner, E. T., Bonitz, R. G., Melko, J. P., Sharaishi, L. R., and Leger, C., 2005. "The Mars Exploration Rover instrument positioning system". In Proceedings of the 2005 IEEE Aerospace Conference.
- [4] Bonitz, R., Shariashi, L., Robinson, M., Carsten, J., Volpe, R., Trebi-Ollennu, A., Arvidson, R., Chu, P., Wilson, J., and Davis, K., 2009. "The Phoenix Mars Lander robotic arm". In Proceedings of the 2009 IEEE Aerospace Conference.
- [5] Kyle, S. A., 1995. "Optical methods for calibrating and inspecting robots". *Computing & Control Engineering Journal*, **6**(4), August, pp. 166–173.
- [6] Wu, C. H., and Lee, C. C., 1985. "Estimation of the accuracy of a robot manipulator". *IEEE Transactions on Automatic Control*, **AC-30**(3), March, pp. 304–306.
- [7] Roth, Z. S., Mooring, B. W., and Ravani, B., 1987. "An overview of robot calibration". *IEEE Journal of Robotics and Automation*, **RA-3**(5), October, pp. 377–385.
- [8] Hayati, S., Tso, K., and Roston, G., 1988. "Robot geometry calibration". In 1988 IEEE International Conference on Robotics and Automation, Vol. 2, pp. 947–951.
- [9] Karan, B., and Vukobratović, M., 1994. "Calibration and accuracy of manipulation robot models - an overview". *Mechanism and Machine Theory*, **29**(3), pp. 479–500.
- [10] Alici, G., and Shirinzadeh, B., 2005. "Enhanced stiffness modeling, identification and characterization for robot manipulators". *IEEE Transactions on Robotics and Automation*, **21**(4), August, pp. 554–564.
- [11] Billing, R., and Fleischner, R., 2011. "Mars Science Laboratory robotic arm". In 14th European Space Mechanisms & Tribology Symposium - ESMATS 2011.
- [12] Craig, J., 1989. *Introduction to Robotics: Mechanics and Control*, 2nd. ed. Addison-Wesley Publishing Company.
- [13] Murray, R., Li, Z., and Sastry, S., 1994. *A Mathematical Introduction to Robotic Manipulation*. CRC Press, Ann Arbor.
- [14] Tsai, L., 1999. *Robot Analysis: The Mechanics of Serial and Parallel Manipulators*. John Wiley & Sons, New York.